Journal of Materials Chemistry A

Accepted Manuscript

ROYAL SOCIETY OF CHEMISTRY

www.rsc.org/materialsA

Journal Name

ARTICLE

Pt-decorated highly porous flower-like Ni particles with high mass activity for ammonia electro-oxidation

Received 00th January 20xx,
Accepted 00th January 20xx

DOI: 10.1039/x0xx00000x

www.rsc.org/

Jie Liu,[a] Bin Chen,[c] Yue Kou,[a] Zhi Liu,[c] Xu Chen,[c] Yingbo Li,[a] Yida Deng,[b] Xiaopeng Han,[a] Wenbin Hu[a,b,c] and Cheng Zhong[*a,b]

Pt-decorated Ni particles with different surface morphologies were directly prepared on the conducting substrate for the use of electrocatalysts for ammonia electro-oxidation. The whole preparation process avoided the use of surfactants, binders, reducing and capping agents. Flower-like Ni particles consisting of interconnecting thin nanosheets and featureless Ni particles with relatively smooth surface were obtained by controlling the electrodeposition potential. Pt-decorated Ni particles were prepared by the galvanic replacement reaction between Ni particles and Pt^{2+} ions. The surface morphology and chemical composition of Pt-decorated Ni particles were characterized by scanning electron microscopy, transmission electron microscopy and X-ray photoelectron spectroscopy. The Pt loading was determined by an inductively coupled plasma method, and the electrocatalytic activity of the prepared electrocatalysts was characterized by cyclic voltammetry. The results showed that there is a significant effect of the surface morphology of Ni particles and the Pt replacement time on the electrocatalytic activity. In particular, Pt-decorated flower-like Ni particles with highly porous structure exhibit a high mass activity of 75.32 mA mg^{-1}, which was 2 times higher than the commercial Pt/C catalysts. The improved activity is attributed not only to the highly porous flower-like morphology, but also to the presence of nanopores and small 2–3 nm sized Pt grains with good dispersion on the petals of flower-like particles.

Introduction

From both energy and environmental point of view, electro-oxidation of ammonia has attracted great attention for various important applications such as ammonia-based fuel cells,[1-4] on-board production of high-purity hydrogen,[5,6] electrochemical removal of ammonia[7,8] and the ammonia detection[9] for environmental protection. As a carbon-free chemical energy carrier, ammonia has high hydrogen storage capacity of 17.7 wt.% and energy density of 3000 Wh kg^{-1}.[10] Therefore, compared to other fuel cells based on organic small molecules such as methanol, ethanol and formic acid, direct ammonia fuel cells have a distinct advantage of no CO_2 emission during the operation (only N_2 and water are produced).[8] In addition, Botte et al.[5-7,11] proposed that ammonia electro-oxidation technology could be used to produce high-purity hydrogen and simultaneously to remove ammonia contaminants in wastewater. Vitse et al.[5] suggested that electrolysis of ammonia requires theoretically 95% less energy than electrolysis of water for hydrogen production. Several critical reviews including the work from our group compared ammonia with other fuels including hydrogen and concluded that ammonia provides an attractive alternative for clean energy supply.[1,12,13]

To date, a wide variety of transition metals (Pt, Pd, Rh, Ru and Ir) and coinage metals (Cu, Ag, and Au) have been studied as electrocatalysts for ammonia electro-oxidation and Pt has been so far regarded as the most effective electrocatalyst.[14-16] However, the high cost and rare resource severely limit the large-scale applications of Pt. Therefore, significant effort has been devoted to developing Pt-based electrocatalysts that can improve the electrocatalytic activity and simultaneously lower the Pt loading.[12,17] The catalytic activity of Pt-based electrocatalysts strongly depends on their surface-to-volume ratio (size),[18-20] shape/morphology,[14,21-25] and composition.[14,22,26] Consequently, great attention has been paid to preparing Pt-based electrocatalysts with various shapes/morphologies to both improve the electrocatalytic activity and reduce the cost. A wide variety of shapes/morphologies, such as zero-dimensional (e.g., nanocubes and nanooctahedrals),[21,24] one-dimensional (e.g., nanowires and nanotubes),[27,28] two-dimensional (e.g., nanobelts and nanosheets),[20,29] and three-dimensional (e.g., nanoflower and nanodendrites) Pt structures,[25,30-32] have been reported. Among these shapes/morphologies, flower-like

[a] Key Laboratory of Advanced Ceramics and Machining Technology (Ministry of Education), School of Materials Science and Engineering, Tianjin University, Tianjin 300072, China. E-mail: cheng.zhong@tju.edu.cn
[b] Tianjin Key Laboratory of Composite and Functional Material, school of Materials Science and Engineering, Tianjin University, Tianjin 300072, China
[c] State Key Laboratory of Metal Matrix Composites, School of Materials Science and Engineering, Shanghai Jiao Tong University, Shanghai, 200240, China

morphologies with a branched structure have received particular interest for electrocatalysis applications.[30,31,33-37] Flower-like Pt particles have been reported to have a high specific activity (activity normalized by the effective surface area) due to their high surface roughness and high density of active sites such as atomic steps, edges and kinks on the branches.[25,30-32,38-42] Besides, the enhanced electric field induced by the tips and sharp edges of the branched flower-like particles may also contribute to the high specific activity.[25,43] Previous work found that flower-like Pt-based particles with highly branched structures showed an improved specific activity for various important electro-oxidation reactions such as the methanol oxidation,[23,30,31,44,45] ethanol oxidation,[37] formic acid oxidation,[30,46] ammonia oxidation,[25,32] glucose electro-oxidation[47] and oxygen reduction reaction.[39,48] For example, Zhang et al.[49] found that the peak current density of methanol oxidation on flower-like Pt particles (about 500 nm size) was about 4.4 times of that on Pt particles with irregular morphology. Previous work from our group also found that the specific activity of rough flower-like Pt particles is nearly 2 times higher than that of smooth Pt particles for ammonia oxidation.[25,32] However, these reported flower-like Pt particles have relatively large particle size (about 100 to 500 nm) and are composed of pure Pt with high Pt loading,[25,30,31,35,37,43,47,49] which strongly limits the surface-to-volume ratio and thus decreases the mass activity (activity normalized by the Pt loading).

The aim of the present work is to effectively improve the Pt utilization degree while preserving the advantages of flower-like morphology. In this work, cost-effective materials, i.e., flower-like Ni particles, were prepared as the support for Pt electrocatalysts in order to significantly reduce the Pt loading. Most flower-like Ni particles were fabricated by wet chemical methods,[50-52] and requires mixing thoroughly with binders and transferring onto a current collector to form an electrode.[53] We proposed a facile, one-step and clean electrodeposition method to prepare flower-like Ni particles directly onto the conducting substrate. Flower-like Ni particles consisting of interconnecting thin nanosheets were formed by simply controlling the electrodeposition potential. Pt-decorated porous flower-like Ni particles were obtained by galvanic replacement reaction of Ni particles with Pt. The whole preparation process is extremely clean since it avoids the use of any surfactants, binders, reducing and capping agents. For the purpose of comparison, featureless Ni particles with relatively smooth surface were also prepared by the electrodeposition method. The effect of surface morphology of Ni particles on the formed Pt-decorated particles was investigated by scanning electron microscopy (SEM), transmission electron microscopy (TEM) and cyclic voltammetry (CV). The exact amount of Pt loading in electrocatalysts was determined by an inductively couple plasma-optical emission spectrometer (ICP-OES) method. To the best of our knowledge, this is the first time to report the preparation of Pt-decorated flower-like Ni particles based on the electrochemical method. Interestingly, this study showed that by carefully controlling the Pt replacement time, the obtained Pt-decorated flower-like Ni particles could exhibit a high mass activity for ammonia electro-oxidation. It is anticipated that this research provides an insight into the development of cost-effective Pt-based electrocatalysts with high activity.

Experimental

Reagents and Materials

K_2PtCl_4 was purchased from Sigma–Aldrich. Na_2SO_4, $NiSO_4$, H_2SO_4, KOH and $(NH_4)_2SO_4$ were purchased from Beijing Chemicals (Beijing, China). All chemicals were of analytical grade and used as received. Indium tin oxide (ITO) glass substrates were purchased from Southern Glass Co., Ltd., Shenzhen, China. Commercial Pt/C catalysts (20 wt.% Pt) were purchased from Johnson Matthey Company. All the solutions were prepared from ultrapure water (18.2 MΩ cm) purified by a Milli-Q water purification system (Millipore, Billerica, MA, USA) and deaerated by purging a high-purity nitrogen (N_2) gas (99.999%) throughout the test.

Electrode Preparation and characterization

Electrodeposition experiments were carried out on a PARSTAT 2273 electrochemical workstation (Princeton Applied Research, USA), using a classical three-electrode cell. An ITO substrate with an exposed geometry surface area of 1 cm^2 was used as the working electrode. A saturated calomel electrode (SCE) and a Pt plate were used as the reference electrode and the counter electrode, respectively. Before use, the ITO substrate was cleaned in acetone and ultrapure water by sonication and dried with a nitrogen stream. Ni particles with different surface morphologies were simply prepared on the ITO substrate by controlling the electrodeposition parameters. Flower-like Ni particles consisting of interconnecting thin nanosheets were prepared by potentiostatic electrodeposition at –1 V(SCE) for 100 s in 0.1 M Na_2SO_4 + 0.02 M $NiSO_4$ solution. For comparison, featureless Ni particles with relatively smooth surface were obtained through potentiostatic electrodeposition at –1 V(SCE) for 10 s followed by –0.6 V(SCE) for 590 s in the same deposition solution. After the electrodeposition, the Ni/ITO electrode was removed from the cell and rinsed with ultrapure water and rapidly transferred into 5 mM K_2PtCl_4 + 0.05 M H_2SO_4 solution. Prepared Ni/ITO electrodes were held in the solution for different times to investigate the effect of the time of the galvanic replacement reaction. Afterwards, the Pt-decorated Ni particles on the electrode was rinsed by ultrapure water and dried in air for further tests. Table 1 shows the sample No. and preparation conditions. For comparison, commercial Pt/C was also used to prepare the electrode. The preparation procedure was shown as follows. 5 mg Pt/C powders were dispersed in 10 mL ethanol solution by sonication for 60 min. 20 μL of ethanol dispersion of Pt/C was then dropped onto a polished glassy carbon electrode with a diameter of 5 mm. After evaporation of the solvent, the electrode was covered with 10 μL of 0.2 wt.% Nafion in ethanol and dried in the air for the following electrochemical tests.

Table 1 Sample No. and the corresponding preparation conditions

Sample No.	Freshly-deposited Ni morphology	Pt replacement time (min)
F-0	Flower-like	—
F-1	Flower-like	1
F-5	Flower-like	5
S-0	Relatively smooth surface	—
S-1	Relatively smooth surface	1
S-5	Relatively smooth surface	5

The surface morphology and structure of Ni or Pt-decorated Ni particles were characterized by a scanning electron microscopy (SEM, S-4800, Hitachi, Japan) and a transmission electron microscopy (TEM) (JEOL-2100F). Elemental analyses for the composition of prepared particles were carried out by an energy dispersive X-ray spectroscope (EDS) equipped on a JEOL-2100F TEM. The crystalline structure of Ni or Pt-decorated Ni particles was characterized by an XRD (BRUKER-AXS) using Cu K_α radiation (λ=0.15406 nm). The surface chemical composition of Ni or Pt-decorated Ni particles was characterized by X-ray photoelectron spectroscopy (XPS), which was performed with a Kratos Axis Ultra^{DLD} spectrometer using an Al K_α source (1486.6 eV). The operating pressure was less than 5×10^{-9} Torr. For analyzing the metal loading of electrolytes, the prepared Pt-decorated Ni electrolytes were fully dissolved by 3 mL aqua regia at 70 °C for 30 min. The aqua regia solution was then diluted with water to 10 mL, and the concentration of Pt and Ni in this solution was analyzed by inductively couple plasma-optical emission spectrometer (ICP-OES, Thermo Scientific, iCAP 6000 series). Based on the concentration of dissolved Pt and Ni in the solution and volume of the solution, the amount (loading) of Pt and Ni in electrocatalysts can be obtained.

Electrochemical measurements

Electrochemical measurements were performed by a PARSTAT 2273 electrochemical workstation, using a classical three-electrode cell. The ITO substrate with Pt-decorated Ni particles on its surface was used as the working electrode. A HgO/Hg reference electrode (filled with 1 M KOH) was used as the reference electrode and a Pt plate was used as the counter electrode. The potential measured by HgO/Hg reference electrode was referred to reversible hydrogen electrode (RHE) for the convenience of comparison. The electrocatalytic activity of Pt-decorated Ni electrocatalysts for ammonia oxidation was characterized by CV measurements in 1 M KOH + 0.1 M ammonia solution at a scan rate of 0.01 V s^{-1}, followed by the chronoamperometric (CA) tests at 0.69 V(RHE) for 3600 s to evaluate the durability. In order to compare the mass activity of Pt-decorated Ni electrocatalysts prepared under different conditions, all the currents in the CV and CA curves were normalized by the Pt loading. All experiments were carried out at controlled temperature of 25±1°C.

Results and discussion

Fig. 1a–c show SEM images of electrodeposited flower-like Ni particles before and after Pt replacement reaction for 1 and 5 min, respectively. As shown in Fig. 1a, freshly deposited flower-like Ni particles consist of interconnecting 2D nanosheets with sharp edges. The assembled nanosheets have a thin thickness, growing anisotropically and extending toward different directions. The time of the galvanic replacement reaction between Ni particles and Pt^{2+} ions plays a significant role in the surface morphology of Pt-decorated Ni particles. When the replacement reaction time is short of 1 min, the Pt-decorated Ni particles are still featured by flower-like morphology (Fig. 1b). However, compared to flower-like pure Ni particles (Fig. 1a), the nanosheets become highly roughen and porous. As the replacement reaction time further increases to 5 min, Pt-decorated Ni particles loses their original flower morphology and are composed of small particles (about 20–30 nm) on the surface due to the extensive replacement between Ni particles and Pt^{2+} ions (Fig. 1c). For comparison, Fig. 1d–f show SEM images of electrodeposited featureless Ni particles with relatively smooth surface before and after Pt replacement reaction for 1 min and 5 min, respectively.

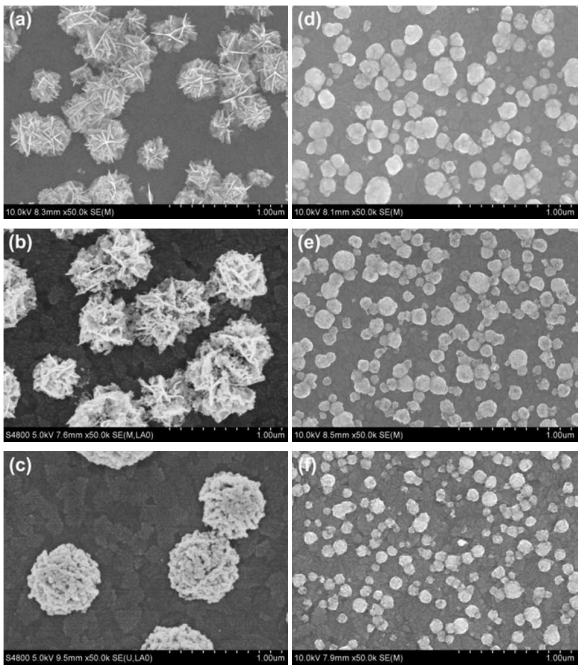

Fig.1 SEM images of (a) flower-like Ni particles electrodeposited at –1 V(SCE) for 100 s in 0.1 M Na_2SO_4 + 0.02 M $NiSO_4$ solution, followed by galvanic replacement reaction between Ni particles and Pt^{2+} ions for (b) 1 min and (c) 5 min; (d) featureless Ni particles electrodeposited at –1 V(SCE) for 10 s followed by –0.6 V(SCE) for 590 s in 0.1 M Na_2SO_4 + 0.02 M $NiSO_4$ solution, followed by galvanic replacement reaction between Ni particles and Pt^{2+} ions for (e) 1 min and (f) 5 min.

Compared to the flower-like Ni particles with porous structure, these featureless Ni particles have relatively smooth surface (Fig. 1d). Short time of galvanic replacement reaction results in the slightly increase of the surface roughness of particles (Fig.1e). With the further increasing in the replacement reaction time, more obvious increased roughness can be observed (Fig. 1f). As the replacement reaction time increases from 1 to 5 min, EDS results show that Pt concentration rises from 2.15 to 9.91 at.% for flower-like Ni particles and it increases from 1.28 to 4.89 at.% for irregular Ni particles. Replacement reaction between flower-like Ni particles and Pt^{2+} ions leads to the higher Pt content than that between irregular Ni particles and Pt^{2+} ions. This can be understood from their morphology difference. Flower-like Ni particles are featured by porous structure with larger surface-to-volume ratio compared to featureless Ni particles with relatively smooth surface. Therefore, flower-like Ni particles provide more active sites for the replacement reaction and thus results in the higher Pt concentration. It should be noted that in the EDS measurement, due to the large penetration depth of X-ray, the effective information depth can be larger than 1 µm. Since the replacement reaction between Ni particles and Pt^{2+} ions is limited to the surface, the formed Pt on the surface contributes only a very small amount of total EDS signal while the inner Ni constitutes most of the total EDS signal. This will be further discussed based on following XPS measurements.

In order to illustrate the effect of electrodeposition potential on the surface morphology of Ni particles, Fig. 2a and b show the chronoamperograms during the electrodeposition of Ni at –1 V(SCE) for 100 s and –1 V(SCE) for 10 s followed by –0.6 V(SCE) for 590 s in 0.1 M Na_2SO_4 + 0.02 M $NiSO_4$ solution, respectively. The different surface morphology of Ni particles electrodeposited at two different conditions can be reflected in the shape and value of the current–time curve. To clearly seen the current variation in Fig. 2b, the inset shows the current–time curve between 11 and 600 s. For both electrodeposition conditions, the current changes sharply in the initial stage, which is related with the double-layer charging and the nucleation process. After the initial change of the electrodeposition current, the chronoamperograms is characterized by a relatively stable current plateau, corresponding to the growth process.[41,54] The value of the current plateau obtained in the electrodeposition at –1 V(SCE) is much higher than that obtained at –0.6 V(SCE). This is attributed to the lower electrodeposition potential of the former, greatly favoring the growth kinetics. It is seen that that surface morphology of Ni particles is related to the value of the electrode current. During the electrodeposition process, there coexist the electro-reduction reaction of Ni ions and the diffusion of Ni ions from the bulk solution towards the electrode surface.[19] At the initial stage of the electrodeposition process, Ni ions are rapidly reduced to Ni atoms, leading to the formation of tiny Ni nuclei. As electrodeposition process proceeds, these Ni nuclei grow into Ni particles. When the electrodeposition potential is low (i.e., electrodeposition overpotential is high), the reduction rate of Ni ions is strongly enhanced under a large cathode current (Fig. 2a). The whole

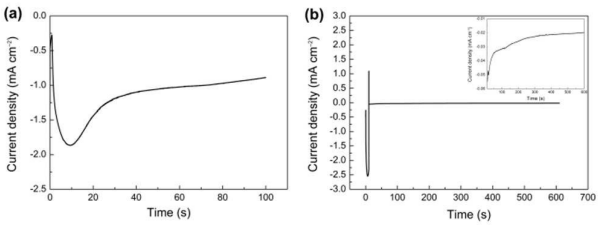

Fig. 2 Chronoamperograms measured during the Ni electrodeposition (a) at –1 V(SCE) for 100 s and (b) at –1 V(SCE) for 10 s followed by –0.6 V(SCE) for 590 s in 0.1 M Na_2SO_4 + 0.02 M $NiSO_4$ solution. The current is normalized to the geometric area of the working electrode.

electrodeposition process is controlled by the diffusion process. As a result, the corner and edge of the Ni nuclei grow quicker than other region, favoring the formation of flower-like particles consisting of interconnecting Ni nanosheets (Fig. 1a). On the contrary, the high electrodeposition potential limits the current for the growth kinetics (Fig. 2b) and thus results in the formation of densely agglomerated structure with relatively smooth surface (Fig. 1d). This phenomenon has also been found for the electrodeposition of Pt, as reported by previous work from our group.[25,32]

Fig. 3 shows XRD pattern of six different samples including flower-like Ni particles (F-0), Pt-decorated flower-like Ni particles prepared by the Pt replacement reaction for 1 min (F-1) and 5 min (F-5), featureless Ni particles with relatively smooth surface (S-0), and Pt-decorated featureless Ni particles prepared by the Pt replacement reaction for 1 min (S-1) and 5 min (S-5). It is seen that all these samples exhibit a similar pattern. The diffraction peaks at 44.5° and 51.9° correspond to (111) and (200) planes of face-centered cubic (fcc) phase of Ni, respectively. It is interesting to note that for all these samples, XRD patterns exhibit the domination of Ni(111) facets. The intensity ratios of the Ni(111) to the Ni(200) diffraction peak range from 3.0 to 3.9 (after subtracting the background signal) for different samples, which are much higher than that of the standard diffraction of Ni powders (1.92).[55] This suggests that the electrodeposited Ni tends to grow with the (111) facets that have the lowest surface free energy (γ) among three low

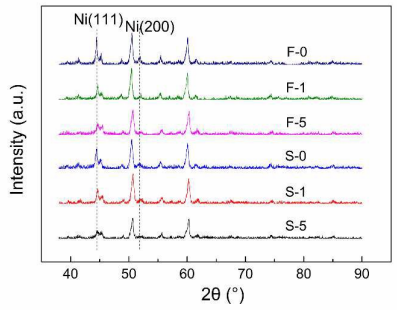

Fig. 3 XRD patterns of six different samples including flower-like and featureless Ni particles, and Pt-decorated Ni particles prepared by different replacement reaction times of 1 and 5 min.

index surfaces (γ(111) < γ(100) < γ(110)[56]). Similar results have been observed for the electrodeposition of Au, as reported by the previous work from our group.[41] The other peaks are the diffraction peaks of ITO. The information depth of X-ray in the XRD measurement is generally on the order of tens of micrometers[57] and therefore contains information mainly from the substrate ITO and Ni. Since the Pt content is very small and limited to the surface of Ni particles, the Pt signal cannot be observed on XRD results.

To investigate the surface composition of prepared particles, Fig. 4a and b show high-resolution XPS spectra of Pt 4f (a) and Ni 2p peaks (b) for flower-like pure Ni particles (F-0) and Pt-decorated flower-like Ni particles obtained by different replacement reaction times of 1 min (F-1) and 5 min (F-5). Fig. 4c and d show high-resolution XPS spectra of Pt 4f (c) and Ni 2p peaks (d) for featureless Ni particles (S-0) and Pt-decorated Ni particles prepared by different replacement reaction times of 1 min (S-1) and 5 min (S-5). XPS is a highly surface-sensitive technique, with an effective information depth of about several nanometers.[57,58] The XPS spectrum of Pt can be divided into two pairs of peaks (Figs. 4a and c). The peaks at 70.4 eV and 73.8 eV are assigned to the binding energies of metallic Pt,[58] the intensities of which are much high than those of peaks at 71.5 eV and 75.5 eV corresponding to PtO or $Pt(OH)_2$.[58,59] This suggests that metallic Pt is the predominant species. In contrast to Pt 4f spectrum, there are shake-up satellites at higher binding energies near the main peaks in Ni 2p spectrum.[58] This feature has also been widely reported by previous studies.[60-62] Furthermore, Ni 2p spectra are relatively complicated depending on the preparation method. In the case of electrodeposited flower-like and featureless Ni particles without the galvanic replacement reaction, measured binding energies of Ni $2p_{3/2}$ and Ni $2p_{1/2}$ locate at 855.7 and 873.1 eV, respectively. Compared to the standard spectrum of metallic Ni, these peaks shift to higher binding energy values and the deconvolution of high-resolution XPS spectra suggests the formation of $Ni(OH)_2$ on the surface.[58,60,62] This is due to the oxidation of the surface of freshly electrodeposited Ni particles. On the contrary, for Ni particles after galvanic replacement by Pt, Ni 2p spectra show different characteristics depending on the surface morphology of Ni particles and the replacement reaction time. For Pt-decorated flower-like Ni particles prepared by short replacement reaction time of 1 min (F-1), the intensities of Ni 2p peaks are significantly lower than the freshly electrodeposited Ni particles (Fig. 4b). Additionally, there is a Ni $2p_{3/2}$ peak at the binding energy of 851.7 eV, corresponding to zero-valent Ni(0) and thus indicating the presence of metallic Ni on the surface.[58] The strong Pt peaks and remarkable decrease of Ni peaks suggest that the surface of flower-like Ni particles is covered by Pt to some extent. The corresponding atomic ratio of Pt and Ni obtained under this condition is 38 : 62 by XPS, which is much larger than the value obtained by EDS measurements. This suggests that the formed Pt by the galvanic replacement is limited to the surface of particles. The surface Pt protects the inner Ni from the oxidation and thus Ni 2p signal corresponding to metallic Ni can be observed, which is different with that for

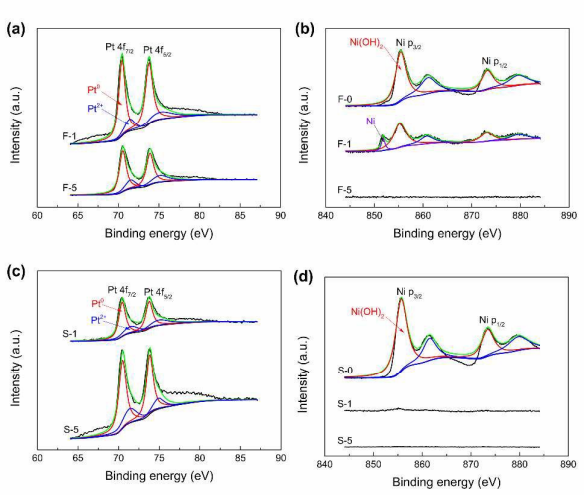

Fig. 4 High-resolution XPS spectra of (a) Pt 4f and (b) Ni 2p peaks for flower-like Ni particles and Pt-decorated flower-like Ni particles obtained by different replacement reaction times of 1 and 5 min; (c) Pt 4f and (d) Ni 2p peaks for featureless Ni particles and Pt-decorated featureless Ni particles prepared by different replacement reaction times of 1 and 5 min.

electrodeposited Ni particles without the galvanic replacement. As the replacement reaction time further increases from 1 to 5 min, the continued covering of flower-like Ni particles by Pt results in the loss of Ni signal (see F-5 in Fig. 4b). However, no obvious Ni signals can be observed for featureless Ni particles after the galvanic replacement by Pt for 1 and 5 min (Fig. 4d). This is in consistence with SEM observations (Fig. 1e and f). Featureless Ni particles have much lower effective surface areas compared to flower-like Ni particles and therefore can be covered by Pt more quickly.

Fig. 5a–c show TEM images with different magnifications and locations of electrodeposited flower-like Ni particles. Due to the formation of nanosheets on the surface, the edge of the Ni particle exhibits a lower contrast ratio than the core of the particle in the TEM image (Fig. 5a). High-magnification TEM

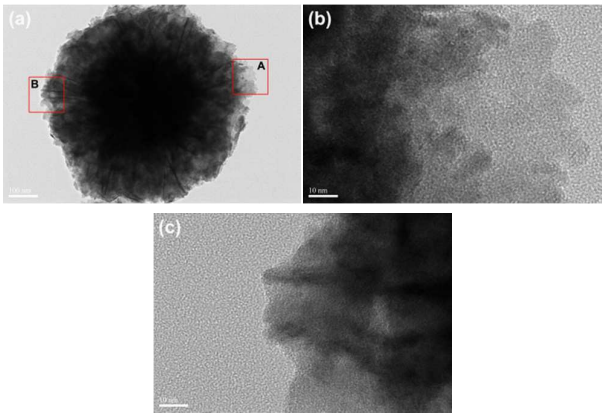

Fig. 5 (a) TEM image of electrodeposited flower-like Ni particles, and high-magnification TEM images of (b) the area marked as A and (c) the area marked as B in Fig. 5(a).

image of the area marked as A in Fig. 5a are shown in Fig. 5b, which clearly shows the presence of thin nanosheets on the surface of flower-like Ni particles. It is seen from Fig. 5b that due to its very thin thickness, the nanosheet shows a very low contrast ratio to the carbon film on the Cu grid for TEM characterizations.[63] High-magnification TEM images of the area marked as B show the feature of the perpendicular nanosheets and their thicknesses are estimated to be about 3 nm (Fig. 5c).

Fig. 6a–c show TEM images with different magnifications and locations of Pt-decorated flower-like Ni particles prepared by Pt replacement for 1 min. The morphology is obviously changed after the galvanic replacement between flower-like Ni particles and Pt ions. Although Pt-decorated Ni particles remain the flower-like morphology for short replacement time, they become significantly porous compared to flower-like Ni particles without replacement reaction. This is in consistence with the SEM characterization (Fig. 1a). By comparing Fig. 5b and 6b, it is seen that the original smooth and continuous nanosheets change to highly porous and discontinuous structure due to the replacement reaction. Because of the larger atomic weight of Pt than Ni, many small nanoparticles with higher contrast ratio are formed on the original nanosheets due to the replacement of Ni by Pt (Fig. 6b). Fig. 6c shows high-magnification TEM image of the area marked as B in Fig. 6a, which contain information of perpendicular nanosheets and can be used to be compared to Fig. 5c. Similar porous structures and the formation of many small nanoparticles can be observed. High-resolution TEM (HRTEM) image shows that these porous nanosheets are composed of many small grains with the diameter about 2–3 nm (Fig. 6d). Besides, nanopores with 2–5 nm size are present on petals of flower-like particles. Fig. 6e shows the elemental mapping of Pt and Ni obtained by energy-dispersive X-ray spectroscopy (EDS) equipped with TEM. Elemental mapping confirms the presence of Pt and Ni elements in Pt-decorated flower-like Ni particles. Since Ni particles are relatively big, the amount of decorated Pt on the surface is extremely low compared to Ni and therefore the Pt signal obtained from EDS is very low. The Pt and Ni loadings for Pt-decorated flower-like Ni particles are 1.5 and 27.8 μg cm^{-2} (normalized by the geometric surface area of the working electrode), respectively. Furthermore, overlaying elemental distribution suggests that Pt is enriched in the outer surface of the particle. This is consistent with the point analysis by EDS for different locations of the particle. It is seen that the EDS result from the core of the particle (Fig. 6f) has a much lower Pt concentration than the edge of the particle (Fig. 6g). Due to the relative large size of Ni particles and small amount of Pt on the surface, the signal of core Ni particles dominantly contributes to the result when EDS is performed in the center of the particle. However, the outer surface of original flower-like Ni particle consists of thin nanosheets (Fig. 1b and Fig. 5b), the galvanic replacement results in the formation of Pt on the surface as revealed by the XPS measurements (Fig. 4). This leads to the higher Pt concentration at the outer part of the particle.

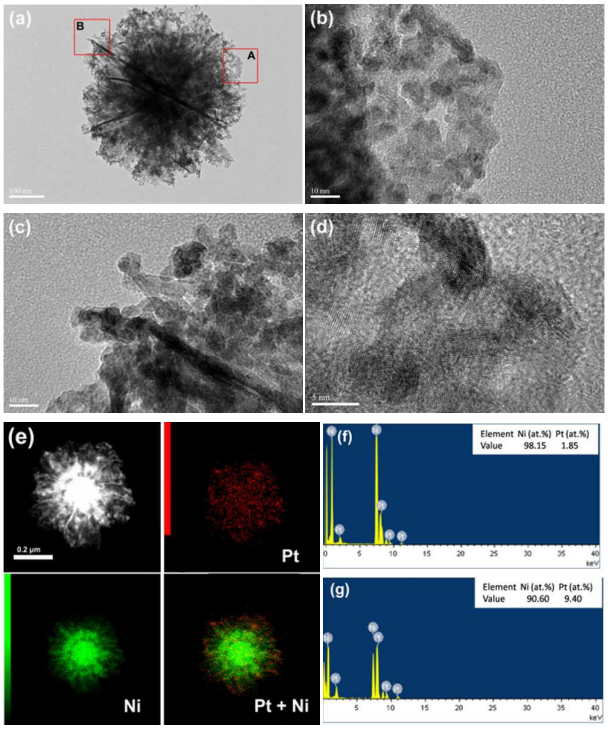

Fig. 6 (a) TEM image of Pt-decorated flower-like Ni particles prepared by galvanic replacement between flower-like Ni particles and Pt^{2+} ions, and high-magnification TEM images of (b) the area marked as A and (c) the area marked as B in Fig. 6(a), and (d) high-resolution TEM image corresponding to the area in Fig. 6(b). (e) Elemental mapping of Pt and Ni for a Pt-decorated flower-like Ni particle, and EDS spectra obtained at (f) the core and (g) the edge of a Pt-decorated flower-like Ni particle.

To understand the effect of the surface morphology of Pt-decorated Ni particles on the electrocatalytic activity of electrocatalysts, Fig. 7a shows the cyclic voltammograms (CVs) of the ammonia electro-oxidation on Pt-decorated Ni particles in 1 M KOH + 0.1 M ammonia solution. To reveal the mass activity, all the currents are normalized by the Pt loading. For the purpose of comparison, CV measured on commercial Pt/C catalysts is also given in Fig. 7a. For Pt-decorated Ni particles, all CVs exhibit a well-defined anodic current peak at around 0.69 V(RHE), which is attributed to the electro-oxidation of ammonia.[64,65] Previous work from our group performed CV measurements in KOH solution without ammonia and did not find such characteristic current peak.[66] Since Ni is inactive toward the electro-oxidation of ammonia,[65] the current of the ammonia electro-oxidation is contributed from the active Pt sites. The peak current density for the ammonia electro-oxidation can generally be used to evaluate the electrocatalytic activity of electrocatalysts. Noticeably, the electrocatalytic activity of Pt-decorated Ni particles is strongly dependent on the surface morphology of Ni particles. This can be seen more clearly in Fig. 7b, which shows the mass activity for different samples. The mass activity is obtained from the peak current density after subtracting the background current in the CV curve in Fig. 7a. Pt-decorated flower-like Ni particles obtained by 1 min galvanic replacement reaction (F-1) has the

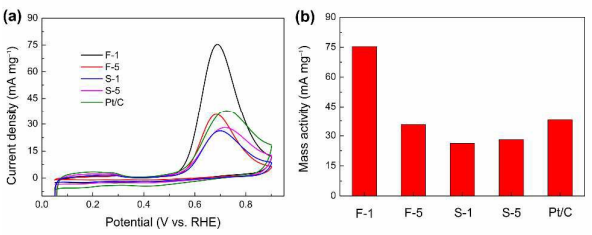

Fig. 7 (a) CVs and (b) mass specific activities of the ammonia electro-oxidation for Pt-decorated flower-like and featureless Ni particles obtained by different replacement reaction times of 1 and 5 min. All currents in CV curves are normalized by the Pt loading.

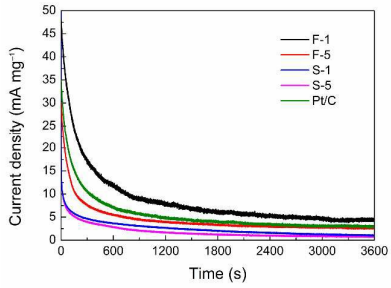

Fig. 8 Chronoamperometric curves of the ammonia electro-oxidation on Pt-decorated flower-like and featureless Ni particles obtained by different replacement reaction times of 1 and 5 min. The electrode potential is 0.69 V(RHE), and all currents are normalized by the Pt loading.

highest mass activity of 75.32 mA mg^{-1} among all the investigated electrocatalysts. This value is 2 times higher than the commercial Pt/C catalysts. Pt-decorated featureless Ni particles obtained by 1 min (S-1) and 5 min (S-5) galvanic replacement reaction show the lowest mass activity (26.28–28.09 mA mg^{-1}). The authors' previous work found that pure Pt (all-Pt) flower-like particles showed the mass activity of 30–47 mA mg^{-1} under the same testing condition,[12,20,25,32] which is much lower than that of the F-1 sample prepared in the present work.

Fig. 8 shows chronoamperometric (CA) curves of the ammonia electro-oxidation on Pt-decorated Ni particles in 1 M KOH + 0.1 M ammonia solution (All currents are normalized by the Pt loadings). The sharp decrease of the current density at the very initial stage is associated with the double-layer charging. The subsequent gradual decay of the current density is due to the consumption of the electroactive species near the electrode surface, which is controlled by the diffusion process. The formation of poisoning species (e.g., N_{ads}) also leads to the decrease of the current density.[16] Compared to other samples, the F-1 sample always gives higher current density throughout the entire 3600 s CA test. At the end of test, the oxidation current density for the F-1 sample is 4.58 mA mg^{-1}, which is much higher than that for other samples (0.77–3.02 mA mg^{-1}). This suggests the higher electrocatalytic activity and stability of Pt-decorated flower-like Ni particles compared to Pt-decorated Ni particles with other morphologies. It has been widely reported that flower-like Pt particles with large number of protruding tips and edges on their surface have higher specific activity for various electro-oxidation reactions such as ammonia and methanol electro-oxidation compared to Pt particles with relatively smooth surface.[19,20,23,25,32] For example, previous studies pointed out that sharp morphology-induced intensification of the electric field could enhance the specific activity of flower-like Pt particles.[25,43] SEM (Fig. 1b) and TEM (Fig. 6a) observations show that the flower-like morphology of original Ni particles can be maintained after short galvanic replacement reaction time of 1 min. Therefore, the flower-like morphology of the F-1 sample is also expected to contribute to the high mass activity. However, this is not the only contributing factor since the mass activity of the F-1 sample is significantly higher than that reported by previous studies concerning flower-like Pt particles under similar testing conditions.[25,32] Due to the Pt replacement and dissolution of replacement and dissolution of Ni during the replacement reaction, original smooth and continues Ni thin nanosheets change to porous structure with the formation of dispersed small Pt grains (2–3 nm size) and nanopores (2–5 nm size), as evidenced by TEM characterizations (Fig. 6b and d). This increases the specific surface area of Pt (i.e., effective surface area normalized by the Pt loading) and thus results in the highest mass activity for ammonia electro-oxidation of F-1 sample among all the investigated samples. However, further increasing in the replacement reaction time results in the growth of Pt into large particles and the loss of flower-like morphology (Fig. 1c). As a result, there is a mass activity loss of the F-5 sample obtained from the flower-like Ni particles followed by the Pt replacement for 5 min.

Finally, the mass activity of the Pt-decorated highly porous flower-like Ni particles (F-1) in the present work is compared to documented electrocatalysts prepared by electrochemical methods, as shown in Table 2. Depending on the preparation methods and testing conditions, the mass activity of documented electrocatalysts ranges from 0.4 to 70 mA mg^{-1}. The value of the mass activity of Pt-decorated porous flower-like Ni particles prepared in this work is the highest (75.32 mA mg^{-1}) among reported values, which is due to the high utilization degree of Pt and morphological contribution.

Table 2 Comparison of the mass activity of electrocatalysts prepared in the present work with previous work for electro-oxidation of ammonia

Electrocatalyst type	Preparation method	Test protocol[a]	Mass activity[b] (mA mg^{-1})	Ref.
Pt-decorated highly porous flower-like Ni particles (this work)	Galvanostatic electrodeposition of Ni followed by Pt	CV in 0.1 M NH_3 + 1 M KOH at 10 mV s^{-1}	75.32	–

	replacement			
Amorphous, boulder-like Pt deposits	Galvanostatic electrodeposition	CV in 1 M NH_3 + 1 M KOH at 10 mV s^{-1}	~22	67
Submicron-sized Pt particles	Galvanostatic electrodeposition	CV in 0.1 M NH_3 + 1 M KOH at 5 mV s^{-1}	0.4~0.5	65
Continuous Pt–Rh layer on carbon fibers	Galvanostatic electrodeposition	CV in 1.03 mM NH_4OH + 0.1 M KOH at 10 mV s^{-1}	~2.9	7
Continuous Pt layer on carbon fibers	Potentiostatic electrodeposition	CV in 5 M KOH containing NH_3 at 5 mV s^{-1}	~6.5	11
Well-dispersed Pt nanosheets	Potentiostatic electrodeposition	CV in 0.1 M NH_3 + 1 M KOH at 10 mV s^{-1}	70	20
Flower-like Pt particles	Potentiostatic electrodeposition	CV in 0.1 M NH_3 + 1 M KOH at 10 mV s^{-1}	30	20
Flower-like Pt particles consisting of Pt nanosheets	Electrodeposition by CV	CV in 0.1 M NH_3 + 1 M KOH at 10 mV s^{-1}	46.8	32
Platinum nanoparticles on nitrogen-doped graphene	Electrodeposition by CV	CV in 0.1 M NH_3 + 1 M KOH at 10 mV s^{-1}	48~71	68

[a] The CV testing was carried out at room temperature.
[b] The value of the mass activity is calculated by the peak oxidation current density normalized by the Pt mass.

Conclusions

Pt-decorated Ni particles with different surface morphologies were directly grown on the conducting substrate to prepare electrocatalysts for ammonia electro-oxidation. The surface morphology of Ni particles can be controlled by a facile electrodeposition method without the use of surfactants and capping agents. Through controlling the electrodeposition potential, flower-like Ni particles consisting of interconnecting thin nanosheets and featureless Ni particles with relatively smooth surface were prepared. Pt-decorated Ni particles were obtained by the galvanic replacement reaction between Ni particles with Pt^{2+} ions. The formation of Pt on the surface of Ni particles was confirmed by XPS. The surface morphology of Ni particles and the time of the replacement reaction play an important role in the mass activity of electrocatalysts. Pt-decorated flower-like Ni particles with highly porous structure exhibit a highest mass activity of 75.32 mA mg^{-1} for ammonia electro-oxidation among all investigated samples, which is 2 times higher than that of commercial Pt/C catalysts. The improved activity of Pt-decorated flower-like Ni particles is attributed not only to the maintenance of the flower-like morphology but also to the formation of nanopores and small 2–3 nm sized Pt grains with good dispersion on the petals of flower-like particles. On the contrary, in the case of Pt-decorated featureless Ni particles with relatively smooth surface, the Pt replacement reaction time does not significantly affect the achieved mass activity and all of them have a low mass activity.

Acknowledgements

This work was supported by the National Natural Science Foundation of China for Distinguished Young Scholars (51125016) and Tianjin Natural Science Foundation.

Notes and references

1 N. V. Rees and R. G. Compton, *Energ. Environ. Sci.*, 2011, 4, 1255-1260.
2 G. T. Fu, C. Liu, R. Wu, Y. Chen, X. S. Zhu, D. M. Sun, Y. W. Tang and T. H. Lu, *J. Mater. Chem. A*, 2014, **2**, 17883-17888.
3 C. L. Zhang, S. Y. Hwang and Z. M. Peng, *J. Mater. Chem. A*, 2013, **1**, 14402-14408.
4 M. H. M. T. Assumpção, S. G. da Silva, R. F. B. De Souza, G. S. Buzzo, E. V. Spinacé, M. C. Santos, A. O. Neto and J. C. M. Silva, *J. Power Sources*, 2014, **268**, 129-136.
5 F. Vitse, M. Cooper and G. G. Botte, *J. Power Sources*, 2005, **142**, 18-26.
6 B. K. Boggs and G. G. Botte, *J. Power Sources*, 2009, **192**, 573-581.
7 E. P. Bonnin, E. J. Biddinger and G. G. Botte, *J. Power Sources*, 2008, **182**, 284-290.
8 F. J. Vidal-Iglesias, J. Solla-Gullón, J. M. Feliu, H. Baltruschat and A. Aldaz, *J. Electroanal. Chem.*, 2006, **588**, 331-338.
9 B. A. L. de Mishima, D. Lescano, T. M. Holgado and H. T. Mishima, *Electrochim. Acta*, 1998, **43**, 395-404.
10 G. Strickland, *Int. J. Hydrogen Energy*, 1984, **9**, 759-766.
11 B. K. Boggs and G. G. Botte, *Electrochim. Acta*, 2010, **55**, 5287-5293.

12 C. Zhong, W. B. Hu and Y. F. Cheng, *J. Mater. Chem. A*, 2013, **1**, 3216-3238.
13 F. Schüth, R. Palkovits, R. Schloegl and D. S. Su, *Energ. Environ. Sci.*, 2012, **5**, 6278-6289.
14 F. J. Vidal-Iglesias, J. Solla-Gullón, V. Montiel, J. M. Feliu and A. Aldaz, *J. Power Sources*, 2007, **171**, 448-456.
15 A. C. A. de Vooys, M. F. Mrozek, M. T. M. Koper, R. A. van Santen, J. A. R. van Veen and M. J. Weaver, *Electrochem. Commun.*, 2001, **3**, 293-298.
16 A. C. A. de Vooys, M. T. M. Koper, R. A. van Santen and J. A. R. van Veen, *J. Electroanal. Chem.*, 2001, **506**, 127-137.
17 S. Zhang, Y. Shao, G. Yin and Y. Lin, *J. Mater. Chem. A*, 2013, **1**, 4631-4641.
18 G. Zhang, C. Huang, R. Qin, Z. Shao, D. An, W. Zhang and Y. Wang, *J. Mater. Chem. A*, 2015, **3**, 5204-5211.
19 C. Zhong, W. B. Hu and Y. F. Cheng, *J. Power Sources*, 2011, **196**, 8064-8072.
20 X. T. Du, Y. Yang, J. Liu, B. Liu, J. B. Liu, C. Zhong and W. B. Hu, *Electrochim. Acta*, 2013, **111**, 562-566.
21 J. A. Michel, W. H. Morris, III and C. M. Lukehart, *J. Mater. Chem. A*, 2015, **3**, 2012-2018.
22 C. Zhong, J. Liu, Z. Y. Ni, Y. D. Deng, B. Chen and W. B. Hu, *Sci. China Mater.*, 2014, **57**, 13-25.
23 J. Liu, C. Zhong, X. Du, Y. Wu, P. Xu, J. Liu and W. Hu, *Electrochim. Acta*, 2013, **100**, 164-170.
24 R. A. Martínez-Rodríguez, F. J. Vidal-Iglesias, J. Solla-Gullón, C. R. Cabrera and J. M. Feliu, *J. Am. Chem. Soc.*, 2014, **136**, 1280-1283.
25 J. Liu, C. Zhong, Y. Yang, Y. T. Wu, A. K. Jiang, Y. D. Deng, Z. Zhang and W. B. Hu, *Int. J. Hydrogen Energy*, 2012, **37**, 8981-8987.
26 X. Zhao, B. Luo, R. Long, C. Wang and Y. Xiong, *J. Mater. Chem. A*, 2015, **3**, 4134-4138.
27 A. Ponrouch, S. Garbarino, E. Bertin, C. Andrei, G. A. Botton and D. Guay, *Adv. Funct. Mater.*, 2012, **22**, 4172-4181.
28 Y. Zuo, K. Cai, L. Wu, T. Li, Z. Lv, J. Liu, K. Shao and H. Han, *J. Mater. Chem. A*, 2015, **3**, 1388-1391.
29 Y. Liu, S. Poyraz, J. H. Xin and X. Zhang, *J. Mater. Chem. A*, 2014, **2**, 7152-7155.
30 Z. Yao, M. Zhu, F. Jiang, Y. Du, C. Wang and P. Yang, *J. Mater. Chem.*, 2012, **22**, 13707-13713.
31 M. Wang, X. Wang, J. Li and L. Liu, *J. Mater. Chem. A*, 2013, **1**, 8127-8133.
32 J. Liu, W. B. Hu, C. Zhong and Y. F. Cheng, *J. Power Sources*, 2013, **223**, 165-174.
33 J. Xu, A. R. Wilson, A. R. Rathmell, J. Howe, M. Chi and B. J. Wiley, *ACS Nano*, 2011, **5**, 6119-6127.
34 S. Sun, D. Yang, D. Villers, G. Zhang, E. Sacher and J. P. Dodelet, *Adv. Mater.*, 2008, **20**, 571-574.
35 M. Zhang, J. J. Lv, F. F. Li, N. Bao, A. J. Wang, J. J. Feng and D. L. Zhou, *Electrochim. Acta*, 2014, **123**, 227-232.
36 A. Mohanty, N. Garg and R. Jin, *Angew. Chem. Int. Edit.*, 2010, **49**, 4962-4966.
37 L. Wei, Y. J. Fan, H. H. Wang, N. Tian, Z. Y. Zhou and S. G. Sun, *Electrochim. Acta*, 2012, **76**, 468-474.
38 P. Song, L. L. He, A. J. Wang, L. P. Mei, S. X. Zhong, J. R. Chen and J. J. Feng, *J. Mater. Chem. A*, 2015, **3**, 5321-5327.
39 G. Fu, K. Wu, J. Lin, Y. Tang, Y. Chen, Y. Zhou and T. Lu, *J. Phys. Chem. C*, 2013, **117**, 9826-9834.
40 B. Lim and Y. Xia, *Angew. Chem. Int. Edit.*, 2011, **50**, 76-85.
41 J. Liu, B. Chen, Z. Ni, Y. Deng, X. Han, W. Hu and C. Zhong, *ChemElectroChem*, 2016, **3**, 537-551.
42 Z. Y. Zhou, Z. Z. Huang, D. J. Chen, Q. Wang, N. Tian and S. G. Sun, *Angew. Chem. Int. Edit.*, 2010, **49**, 411-414.
43 J. Liu, X. Wang, Z. Lin, Y. Cao, Z. Zheng, Z. Zeng and Z. Hu, *Electrochim. Acta*, 2014, **136**, 66-74.
44 X. M. Chen, B. Y. Su, G. H. Wu, C. J. Yang, Z. X. Zhuang, X. R. Wang and X. Chen, *J. Mater. Chem.*, 2012, **22**, 11284-11289.
45 Y. Chen, J. Yang, Y. Yang, Z. Peng, J. Li, T. Mei, J. Wang, M. Hao, Y. Chen, W. Xiong, L. Zhang and X. Wang, *Chem. Commun.*, 2015, **51**, 10490-10493.
46 M. Gong, F. Li, Z. Yao, S. Zhang, J. Dong, Y. Chen and Y. Tang, *Nanoscale*, 2015, **7**, 4894-4899.
47 L. Su, W. Jia, L. Zhang, C. Beacham, H. Zhang and Y. Lei, *J. Phys. Chem. C*, 2010, **114**, 18121-18125.
48 X. Yu, H. Wang, L. Guo and L. Wang, *Chem.-Asian J.*, 2014, **9**, 3221-3227.
49 H. Zhang, W. Zhou, Y. Du, P. Yang and C. Wang, *Electrochem. Commun.*, 2010, **12**, 882-885.
50 J. Xiong, H. Shen, J. Mao, X. Qin, P. Xiao, X. Wang, Q. Wu and Z. Hu, *J. Mater. Chem.*, 2012, **22**, 11927-11932.
51 Y. Wang, Q. Zhu and H. Zhang, *Mater. Res. Bull.*, 2007, **42**, 1450-1456.
52 B. Zhao, G. Shao, B. Fan, B. Sun, K. Guan and R. Zhang, *J. Mater. Sci. -Mater. Electron.*, 2014, **25**, 3614-3621.
53 G. Zhang, W. Li, K. Xie, F. Yu and H. Huang, *Adv. Funct. Mater.*, 2013, **23**, 3675-3681.
54 H. H. Hsu, P. R. Selvaganapathy and L. Soleymani, *J. Electrochem. Soc.*, 2014, **161**, D3078-D3086.
55 H. Chen, C. Xu, C. Chen, G. Zhao and Y. Liu, *Mater. Res. Bull.*, 2012, **47**, 1839-1844.
56 W. Luo, W. Hu, K. Su and F. Liu, *Appl. Surf. Sci.*, 2013, **265**, 375-378.
57 X. Chen, P. A. Glans, X. Qiu, S. Dayal, W. D. Jennings, K. E. Smith, C. Burda and J. Guo, *J. Electron. Spectrosc. Relat. Phenom.*, 2008, **162**, 67-73.
58 J. F. Moulder, W. F. Stickle, P. E. Sobol and K. D. Bomben, *Handbook of X-ray Photoelectron Spectroscopy*, Minnesota: Perkin-Elmer Corporation, 1992.
59 T. C. Deivaraj, W. Chen and J. Y. Lee, *J. Mater. Chem.*, 2003, **13**, 2555-2560.
60 X. Chen, S. Chen, C. Lin, Z. Jiang and W. Shangguan, *Int. J. Hydrogen Energy*, 2015, **40**, 998-1004.
61 S. Du, Y. Lu, S. K. Malladi, Q. Xu and R. Steinberger-Wilckens, *J. Mater. Chem. A*, 2014, **2**, 692-698.
62 I. Mintsouli, J. Georgieva, E. Valova, S. Armyanov, A. Kakaroglou, A. Hubin, O. Steenhaut, J. Dille, A. Papaderakis, G. Kokkinidis and S. Sotiropoulos, *J. Solid State Electrochem.*, 2013, **17**, 435-443.
63 W. Ni, B. Wang, J. Cheng, X. Li, Q. Guan, G. Gu and L. Huang, *Nanoscale*, 2014, **6**, 2618-2623.
64 J. Galipaud, C. Roy, M. H. Martin, S. Garbarino, L. Roué and D. Guay, *ChemElectroChem*, 2015, **2**, 1187-1198.
65 K. Yao and Y. F. Cheng, *J. Power Sources*, 2007, **173**, 96-101.

66 X. H. Deng, Y. T. Wu, M. F. He, C. Y. Dan, Y. J. Chen, Y. D. Deng, D. H. Jiang and C. Zhong, *Acta Chim. Sinica*, 2011, **69**, 1041-1046.
67 M. Cooper and G. G. Botte, *J. Electrochem. Soc.*, 2006, **153**, A1894-A1901.
68 Y. Zhou, G. Zhang, Z. Gong, X. Shang and F. Yang, *ChemElectroChem*, 2016, **3**, 605-614.